





Search for Dark Matter Lines in the gamma-ray energy spectra with the *Fermi*-LAT

M.N. Mazziotta ^{a,*} M. Giliberti ^{a,b} F. Loparco ^{a,b} and D. Serini ^a for the *Fermi*-LAT collaboration

^a*Istituto Nazionale di Fisica Nucleare, Sezione di Bari,
via Orabona 4, I-70126 Bari, Italy*

^b*Dipartimento di Fisica dell'Università e del Politecnico di Bari,
via Amendola 173, I-70126 Bari, Italy*

E-mail: mazziotta@ba.infn.it

Dark matter (DM) in the Milky Way may annihilate or decay directly into gamma rays, producing a monoenergetic line-like excess in the energy spectra. If detected, such features would provide a clear DM signature. In this work, we present an update on line search with 13.75 years of *Fermi* Large Area Telescope (LAT) data from 1 GeV to 1 TeV in five sky regions centered on the Galactic Center, optimized for different DM density profiles and annihilation or decay channels. We improve the fitting procedure by combining the likelihood profiles for different energy dispersion event types (EDISP). To account for systematic uncertainties, we include the data from the control region along the Galactic plane in the fit procedure. We find no statistically significant evidence of features in our data, and set constraints on the velocity-averaged DM annihilation cross sections and on the DM decay time. Compared to the previous *Fermi*-LAT results, the limits on the DM parameters at 95% confidence level in the low energy band are even stronger up to 1-2 orders of magnitude depending on the sky region, thanks to the improved analysis method.

38th International Cosmic Ray Conference (ICRC2023)
26 July - 3 August, 2023
Nagoya, Japan



*Speaker

1. Introduction

While the existence of Dark Matter (DM) is very well established by the scientific community, the debate on its nature is still open. Weakly Interacting Massive Particles (WIMPs), whose existence is predicted by several theories beyond the Standard Model (SM), are among the most credited DM candidates, since their properties fit with observational constraints [1]. Indirect DM searches with gamma rays aim at the detection of photons eventually produced in processes involving DM particles, which are expected to exhibit characteristic spectral features. These searches are performed looking at astrophysical targets where DM is most expected to exist.

Our Galaxy is thought to be embedded in a spherical DM halo and is therefore a favorable target for DM searches. A possible DM signature in gamma rays would be the detection of a spectral line, which would result from WIMP self-annihilations ($\chi\chi \rightarrow \gamma\gamma$) or decays ($\chi \rightarrow \gamma\gamma$), as WIMPs in the Milky Way are assumed to be non-relativistic ($v/c \sim 10^{-3}$). In the first case, the gamma-ray line would appear at the WIMP mass m_χ , while in the second case the line would appear at a mass $m_\chi/2$. This line-like feature would stand out prominently and would be a smoking gun for DM annihilation and decay processes, since no other astrophysical mechanisms are known to produce such a sharp feature in the gamma-ray spectrum from our Galaxy.

The expected gamma-ray differential flux from a sky region covering a solid angle $\Delta\Omega$ centered on a DM source can be calculated, for the self-annihilation¹ and decay processes, as [2]:

$$\left(\frac{d\Phi}{dE}\right)_{ann} = \frac{1}{4\pi} \frac{\langle\sigma_{ann}v\rangle_{\gamma\gamma}}{2m_\chi^2} \left(\frac{dN_\gamma}{dE}\right)_{ann} J_{ann}(\Delta\Omega) \quad (1)$$

$$\left(\frac{d\Phi}{dE}\right)_{decay} = \frac{1}{4\pi} \frac{1}{m_\chi\tau} \left(\frac{dN_\gamma}{dE}\right)_{decay} J_{decay}(\Delta\Omega) \quad (2)$$

where $\langle\sigma_{ann}v\rangle_{\gamma\gamma}$ is the velocity-averaged WIMP annihilation cross section into gamma rays and τ is the WIMP decay time, the so-called J-factors, $J_{ann}(\Delta\Omega)$ and $J_{decay}(\Delta\Omega)$, depend on the amount of DM along the line of sight.

In this work, we search for possible gamma-ray spectral lines from our Galaxy using the data collected by the Large Area Telescope (LAT) on board the *Fermi* Gamma ray Space Telescope [3]. In the present work we update the results from previous *Fermi*-LAT line searches [4–8] using a 13.75 years data sample processed with the newest Pass 8 event selection [2]. Our analysis covers over three decades in energy and accounts for systematic uncertainties, which are estimated using the Galactic Plane (GP) as control region. In Sec. 2 we illustrate the event selection implemented in this work; in Sec. 3 we describe the data analysis procedure; finally, the results of the analysis are shown in Sec. 4 and are discussed in Sec. 5.

2. Event selection

The dataset used in this analysis consists of 165 months of Pass 8 data from August 4th, 2008 to April 30th, 2022, with photons of the CLEAN event class in the energy range from 100 MeV to 2 TeV, converting either in the front or in the back sections of the Tracker (F+B) [2].

¹The annihilation yield of DM is evaluated under the assumption that the particle χ is of Majorana type, i.e. coincides with its antiparticle; otherwise, an additional factor of 1/2 should be included in Eq. 1.

We select events with zenith angle less than 100° , in order to reject photons from the bright Earth's limb. We also restrict the time intervals (“Good Time Intervals”, GTIs) to the periods when the LAT was operating in its standard science operation configuration and was outside the South Atlantic Anomaly (SAA).

Within the selected event sample, the subsamples corresponding to different event types (EDISP0, EDISP1, EDISP2, EDISP3) in which the class is partitioned are also selected, to perform individual analysis on each subsample and a combined analysis of all the four subsamples.

Following the approach of Ref. [6], we select five different Regions of Interest (ROIs), corresponding to cones with the axis pointing towards the Galactic Center (GC) and with different apertures, which in the following will be labeled as R3 (3° aperture), R16 (16°), R41 (41°), R90 (90°), and R180 (180° , corresponding to the whole sky). A mask, corresponding to the region with Galactic latitude $|b| < 5^\circ$ and Galactic longitude $|l| > 6^\circ$, is applied to all ROIs (with the exception of R3). Each ROI is optimized to enhance the signal-to-noise ratio for different DM density profiles, derived from both simulation studies and mass mapping measurements. While R3, R16, R41 and R90 are all optimized for annihilation processes, R180, which encompasses the entire sky, is optimized for possible decay events.

3. Data analysis

A maximum likelihood fit procedure in sliding energy windows has been implemented to search for possible line-like features in the gamma-ray spectra of the various ROIs. The analysis is performed in the energy interval from 1 GeV to 1 TeV. For each ROI, we analyze the whole event samples, separate analyses are also performed on the subsamples corresponding to the different event types EDISP0, EDISP1, EDISP2 and EDISP3. In addition, a combined analysis of the four event types is also implemented.

The sliding window corresponding to a given energy E is defined as the interval $[E(1 - w), E(1 + w)]$, where wE is the width of the window. The results in this work are obtained by setting $w = 0.50$, which corresponds to a window size larger than the energy resolution of the LAT, which is at most 30% in the worst case (energies around 30 MeV). A possible gamma-ray line at energy E is expected to yield a signal spread over an energy interval with the size of the energy resolution. This signal will, therefore, lie within one of the sliding windows.

The energy interval from 1 GeV to 1 TeV is divided into 32 bins per decade, equally spaced on a logarithmic scale. For each ROI, given the width of the energy windows, we perform up to 96 fits. If less than 10 counts were found in a given energy window, the corresponding fit was not performed because of the poor statistics.

In a given energy window, the photon flux from any of the ROIs can be written as: $\Phi_{tot}(E_t|\vec{\theta}) = \Phi_{bkg}(E_t|\vec{\theta}_b) + \Phi_{sig}(E_t|\vec{\theta}_s)$ where $\Phi_{sig}(E_t|\vec{\theta}_s)$ and $\Phi_{bkg}(E_t|\vec{\theta}_b)$ are the signal and background fluxes respectively, while $\vec{\theta} = (\vec{\theta}_b, \vec{\theta}_s)$ are the parameters of the model. The signal flux is the possible line-like feature originated from DM and is given by $\Phi_{sig}(E_t|s) = s\delta(E_t - E_{line})$, where the parameter $s \geq 0$ represents the line intensity and δ is the Dirac delta function. The background flux can be seen as the sum of a “smooth” contribution $\Phi_{bkg,smooth}(E_t)$, originated from the steady gamma-ray emission from known astrophysical processes, and from a possible additional line-like contribution $\Phi_{bkg,line}(E_t)$, which could mimic a DM feature, and is originated

from instrumental (systematic) effects. The smooth component of the background flux is described with a simple power law in the energy region above 10 GeV ($\Phi_{bkg,smooth}(E_t) = k(E_t/E_0)^{-\Gamma}$ where $E_0 = 1$ GeV is a scale energy), and with a log-parabola in the region below 10 GeV ($\Phi_{bkg,smooth}(E_t) = k(E_t/E_0)^{-\Gamma-\beta \log(E/E_0)}$). The log-parabola accommodates the presence of a curvature in the gamma-ray fluxes at low energies, which cannot be accounted for by the simple power law. Finally, the line-like background component is given by $\Phi_{bkg,line}(E_t|b) = b\delta(E_t - E_{line})$ where b is the line intensity, which can be either positive or negative, since the background line is associated to any instrumental effects (systematic uncertainties).

To disentangle the possible line contribution due to the systematic effects from that of a potential DM signal, we also fit the counts in a control region, corresponding to the part of the GP which was masked (see Sec. 2). The photon flux in the control region is only due to background and is given by $\Phi_{GP}(E_t|\vec{\theta}_b) = \Phi_{GP,smooth}(E_t) + \Phi_{bkg,line}(E_t)$, where $\Phi_{GP,smooth}$ is the smooth component of the flux, modeled in a similar way as the smooth component of the background flux.

The expected photon counts in each energy bin for each ROI (or in the control region) can be evaluated by folding the flux models with the exposures, and are given by $\mu_j = \int dE_t \mathcal{E}_{ROI}(E_j|E_t) \Phi(E_t)$, where $\mathcal{E}_{ROI}(E_j|E_t)$ is the exposure of the ROI (control region), which depends on true (E_t) and observed (E_j) energies, and $\Phi(E_t)$ is the appropriate photon flux.

In the null hypothesis, a background-only model is assumed, i.e., $\Phi_{sig} = 0$, which corresponds to $s = 0$; in the alternative hypothesis, the presence of a signal is assumed, i.e., $\Phi_{sig} > 0$, which corresponds to $s > 0$. For each of the two hypotheses, it is possible to define a Poisson likelihood function. In particular, we define the log-likelihood ratios as $-2 \ln \lambda(\vec{\theta}) = -2 \sum_j \left[-\mu_j + n_j - n_j \ln \left(\frac{n_j}{\mu_j} \right) \right]$, where $\vec{n} = (n_1, n_2, \dots)$ is the vector of the observed counts in each energy bin, while $\vec{\mu}(\vec{\theta}) = (\mu_1(\vec{\theta}), \mu_2(\vec{\theta}), \dots)$ is the corresponding vector of the expected counts, which depends on the set of parameters $\vec{\theta}$ in the model. The index j runs over the energy bins belonging to the fit window of the signal ROI and of the control region. The fit parameters are $\vec{\theta} = (k_{ROI}, \Gamma_{ROI}, \beta_{ROI}, k_{GP}, \Gamma_{GP}, \beta_{GP}, b, s)$. The null hypothesis is nested in the alternative hypothesis, since its model can be obtained from the general model by setting $s = 0$.

We also implement a procedure to combine the likelihood functions for the subsamples with EDISP0, EDISP1, EDISP2 and EDISP3. The "combined likelihood" is defined as the product of individual likelihood functions associated to the different event types in a given ROI, i.e.: $\lambda_{combined} = \prod_i \lambda_i(s)$, where i is the index referred to the event types. Also in this case, the function $-2 \ln \lambda_{combined}$ is studied.

Figure 1 shows a comparison among the profiles of the likelihood functions for the different event types EDISP0, EDISP1, EDISP2, EDISP3 and for the combined analysis, for a line at energy $E_{line} = 4.8$ GeV. The curve obtained from the combined analysis decreases more quickly than those obtained from individual analyses of different event types, thus yielding stronger constraints on the line intensity.

The alternative hypothesis, H_1 , is tested against the null hypothesis, H_0 , using the likelihood functions λ_1 and λ_0 . The fitted signal line strength is the value of s corresponding to the maximum of λ_1 . The test statistics is defined as $TS = 2[\ln \lambda_{1,max} - \ln \lambda_{0,max}]$ where $\lambda_{1,max}$ and $\lambda_{0,max}$ are the maximum likelihood ratios for the hypothesis H_1 and H_0 respectively. Since λ_1 contains one additional parameter with respect to λ_0 , the TS is expected to follow a χ^2 distribution with

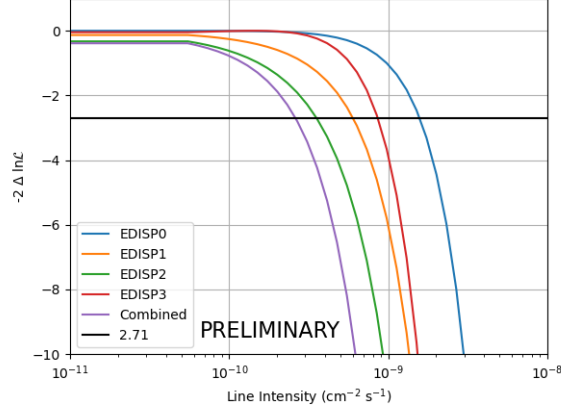


Figure 1: Profile of $-2\Delta\ln\mathcal{L}$, evaluated for the different event types as a function of the line intensity s at $E_{line} = 4.8$ GeV. The ULs at 95% CL are determined by the intersection of the curves with the horizontal black line at $-2\Delta\ln\mathcal{L} = -2.71$. The combined procedure yields stronger constraints (purple line) than the analyses of individual event types.

1 degree of freedom. A feature is considered (locally) significant if the TS exceeds a threshold value corresponding to the required level of significance (the significance level in σ units is given by \sqrt{TS}). If a line is not significant, the upper limits (UL) at 95% confidence level (CL) on its intensity s can be evaluated by searching the value of s for which $TS = TS_{min} + 2.71$, where $TS_{min} = TS(s_{min})$ is the TS of the fit.

A set of 1000 background-only Monte Carlo simulations (pseudoeperiments) is performed to study the sensitivity of the present analysis to the null hypothesis. Each pseudoeperiment is generated starting from a template of the count distributions corresponding to the null hypothesis. The counts in each energy bin are extracted from a Poisson distribution with its average value taken from the template model. The same analysis chain as for real data is then been to the simulated data. The distributions of the TS values and of the ULs on the line intensities obtained from the pseudoeperiments for each value of the line energy are then studied.

4. Results

Figure 2 shows the TS obtained in the combined analysis of the different event types EDISP0, EDISP1, EDISP2 and EDISP3 compared to the expectations from the pseudoeperiments in each of the 5 ROIs. The 68% and 95% containment bands are evaluated from the quantiles of the TS distributions. Almost all the measured TS values lie within the expectation bands from the pseudoeperiments, with a few outliers. In R3, R16 and R41, a feature with $TS \sim 7.5$ at ~ 4 GeV is found. The features with the highest TS ($\sim 12.5 - 14$) are found at the lower edge of the fit range (~ 1 GeV) in R90 and R180.

The data analysis has been implemented in sliding energy windows, which are correlated. To verify whether the outliers in Fig. 2 correspond to significant features, a global significance indicator is needed, which takes into account the effective number of trials. To evaluate the global significance, we analyze the results of the pseudoeperiments discussed in Sec. 3. For

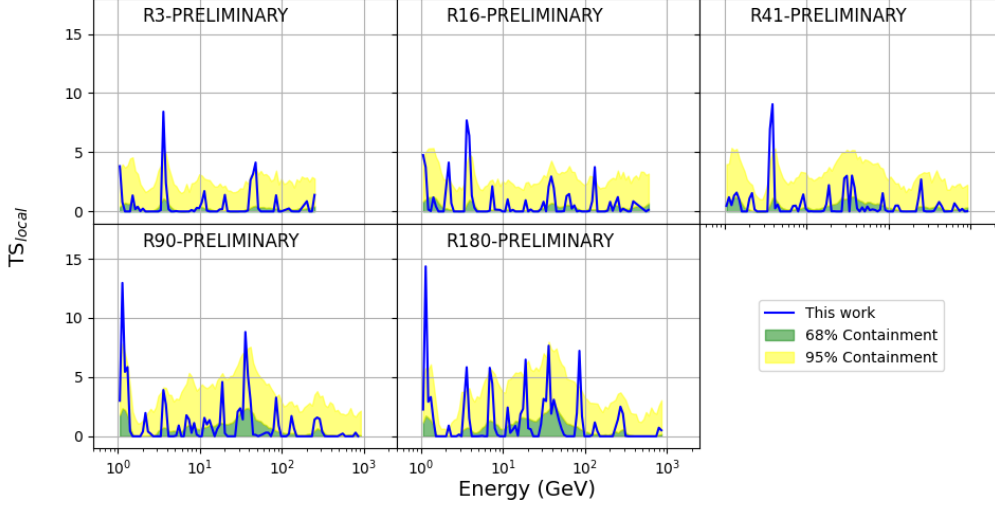


Figure 2: Local TS as a function of energy in R3, R16, R41 and R180 for the combined analysis. The green and yellow bands show the 68% and 95% expected containment bands derived from 1000 background-only pseudoexperiments.

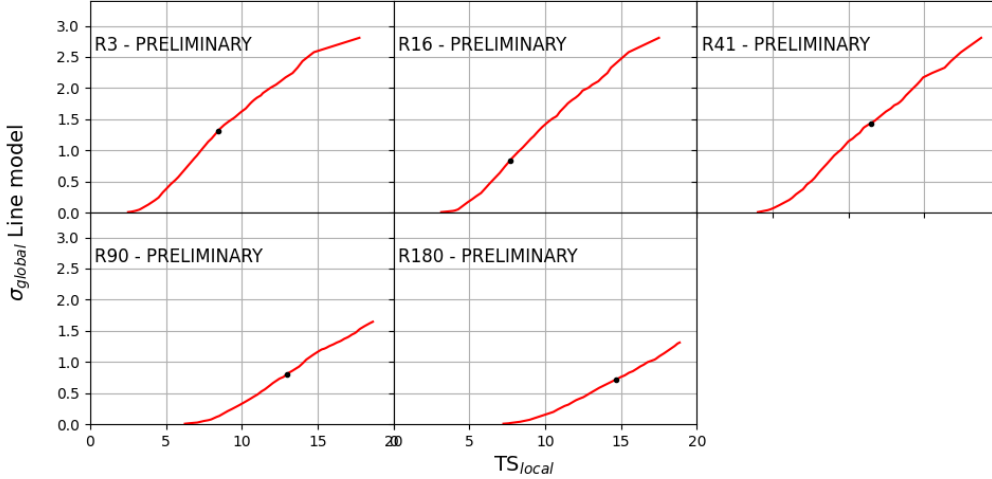


Figure 3: Global significance s_{global} as a function of the local TS in R3, R16, R41 and R180. The black dots represent the maximum TS values coming from our data set analysis.

each ROI, we build therefore the distribution of the maximum TS_{max} obtained in the pseudoexperiments, and we evaluate its quantiles. Assuming that the global significance obeys a half-normal distribution, we associate a global significance to each value of TS , obtaining the plots shown in Fig. 3. We see that the potential feature with the highest global significance is found in R41, but its global significance is $\sim 1.5\sigma$, deeming the signal globally insignificant.

Since all potential features are not globally significant, we evaluate ULs on the line intensities. Fig. 4 shows the ULs at 95% CL on the line intensity as a function of the line energy for the combined analysis. Figure 4 also shows the 68% and 95% containment bands, evaluated from

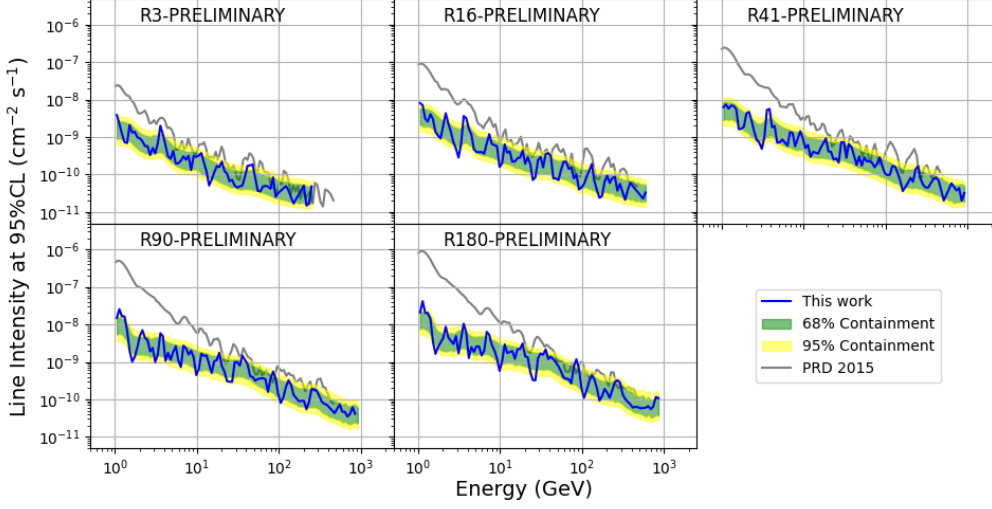


Figure 4: ULs on the line intensity at 95% CL in R3, R16, R41 and R180 for the combined analysis. The green and yellow bands show the 68% and 95% expected containment bands derived from 1000 background-only pseudoexperiments. The limit obtained in ref. [8] in the same ROIs are also shown (grey line).

the distributions of the ULs obtained in the pseudoexperiments. The measured ULs lie within the containment bands, and are therefore consistent with the expectations for the null hypothesis.

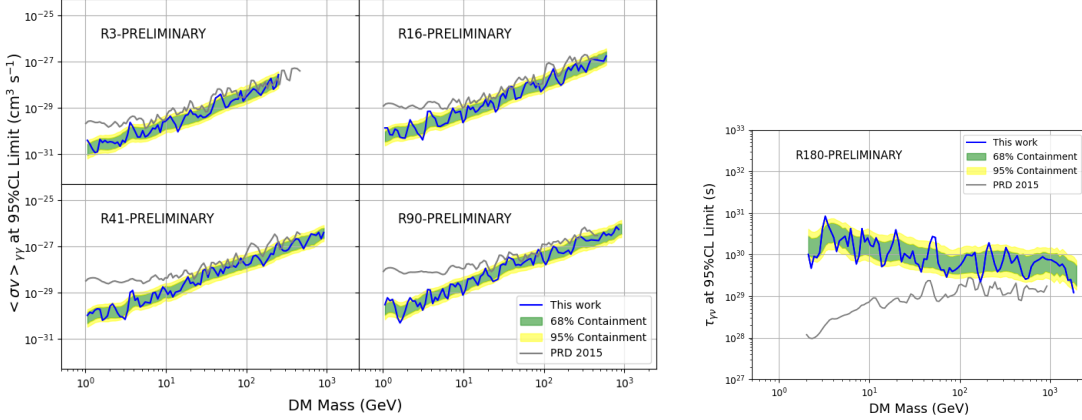


Figure 5: Left panel: Upper limit at 95% CL on the $\langle\sigma_{ann}v\rangle$ as a function of DM mass from the analysis of R3, R16, R41 and R90. Right panel: Lower limit at 95% CL on the decay time τ as a function of DM mass from the analysis of R180. The green and yellow bands show the 68% and 95% expected containment bands derived from 1000 background-only pseudoexperiments. The limits in Ref. [8] are also shown.

5. Discussion and conclusions

The ULs on the parameter s can be converted into ULs on the velocity-averaged annihilation cross section $\langle\sigma_{ann}v\rangle$ or into lower limits on the DM decay time τ (in the case of R180).

These constraints are shown in Figure 5, where the containment bands obtained from the pseudo-experiments are also shown. The limits are compared with the results of Ref. [8]. At low energies (1-10 GeV), the limits obtained in this analysis are a factor ~ 100 stronger than those obtained in ref. [8] (grey line), while at higher energies this work's limits are slightly better. The improvement at low energies is due to not only the use of the combined likelihood analysis technique, but also to the use of a more accurate model of the smooth component of the background flux.

Acknowledgements

The *Fermi*-LAT Collaboration acknowledges support for LAT development, operation and data analysis from NASA and DOE (United States), CEA/Irfu and IN2P3/CNRS (France), ASI and INFN (Italy), MEXT, KEK, and JAXA (Japan), and the K.A. Wallenberg Foundation, the Swedish Research Council and the National Space Board (Sweden). Science analysis support in the operations phase from INAF (Italy) and CNES (France) is also gratefully acknowledged. This work performed in part under DOE Contract DE-AC02-76SF00515.

References

- [1] J.L. Feng, *Dark Matter Candidates from Particle Physics and Methods of Detection*, *Ann. Rev. Astron. Astrophys.* **48** (2010) 495 [1003.0904].
- [2] W. Atwood et al., *Pass 8: Toward the Full Realization of the Fermi-LAT Scientific Potential*, 3, 2013 [1303.3514].
- [3] W.B. Atwood et al., *The Large Area Telescope Fermi Gamma-ray Space Telescope mission*, *The Astrophysical Journal* **697** (2009) 1071.
- [4] A.A. Abdo et al., *Fermi Large Area Telescope search for photon lines from 30 to 200 GeV and Dark Matter implications*, *Phys. Rev. Lett.* **104** (2010) 091302.
- [5] M. Ackermann et al., *Fermi LAT search for Dark Matter in gamma-ray lines and the inclusive photon spectrum*, *Phys. Rev. D* **86** (2012) 022002.
- [6] M. Ackermann et al., *Search for gamma-ray spectral lines with the Fermi Large Area Telescope and Dark Matter implications*, *Phys. Rev. D* **88** (2013) 082002.
- [7] A. Albert et al., *Search for 100 MeV to 10 GeV γ -ray lines in the Fermi-LAT data and implications for gravitino dark matter in the $\mu\nu$ SSM*, *Journal of Cosmology and Astroparticle Physics* **2014** (2014) 023.
- [8] M. Ackermann et al., *Updated search for spectral lines from Galactic dark matter interactions with pass 8 data from the Fermi Large Area Telescope*, *Physical Review D* **91** (2015) .
- [9] G. Steigman, B. Dasgupta and J.F. Beacom, *Precise relic WIMP abundance and its impact on searches for dark matter annihilation*, *Physical Review D* **86** (2012) .